Proceedings of the ASME 2013 International Design Engineering Technical Conferences & Computers and Information in Engineering Conference
IDETC/CIE 2013
August 4-7, 2013, Portland, Oregon, USA

DETC2013-13289

DRAFT: AVIAN-INSPIRED GRASPING FOR QUADROTOR MICRO UAVS

Justin R. Thomas
GRASP Lab
University of Pennsylvania
Philadelphia, Pennsylvania, 19104
Email: jut@seas.upenn.edu

Joe J. Polin
Koushil Sreenath
Vijay Kumar
GRASP Lab
University of Pennsylvania
Philadelphia, Pennsylvania, 19104

ABSTRACT

Micro Unmanned Aerial Vehicles (MAVs) have been used in a wide range of applications [1, 2, 3]. However, there are few papers addressing grasping and transporting payloads using MAVs. Drawing inspiration from aerial hunting by birds of prey, we design and equip a quadrotor MAV with an actuated appendage enabling grasping and object retrieval at high speeds. We develop a nonlinear dynamic model of the system, demonstrate that this system is differentially flat, plan dynamic trajectories using the flatness property, and present experimental results with pick-up velocities at 2 m/s (6 body lengths/second) and 3 m/s (9 body lengths/second). Finally, the experimental results with our MAV are compared with observations derived from video footage of a Bald Eagle swooping down and snatching a fish out of water.

INTRODUCTION

Predatory birds have the ability to swiftly swoop down from great heights and grasp prey, with extremely high rates of success, from the ground, water, and air while flying at high speeds [4]. Although recent years have seen much improvement in the capabilities of micro Unmanned Aerial Vehicles (MAVs) [5, 6], such dynamic aerial manipulation, common in nature, is unrivaled among MAVs. The present state-of-art in aerial manipulation ranges from using grippers for construction [1], and cable-suspended loads for dynamic transportation [2]. Acquiring, transporting and deploying payloads while maintaining a significant velocity are important since they would save MAVs time and energy by minimizing required flight time. For example, high-speed grasping could be used in rescue operations where speed and time are critical, and in operations requiring a MAV to quickly swoop down and pickup an object of interest.

FIGURE 1. VIDEO FRAMES OF EAGLE GRASPING PREY [7]

Moreover, the dynamic grasping functionality could also be extended to achieve perching capabilities, which could be used to quickly escape high winds, achieve immediate silence in stealth operations, and improve mission duration by reducing hover time. Particular requirements for grasping and perching are planning of feasible dynamic trajectories and precise control.

With the ever-expanding body of MAV applications, there has also been a rising need for articulated appendages capable of interacting with the environment. Doyle et al. developed a passively actuated gripper to facilitate perching [8]; Lindsey et al. designed a servo-driven claw to transport plastic construction beams [1]; and Mellinger et al. utilized a gripper with fish hooks to pierce its targets [9]. In the same spirit, Dollar et al. developed fingers that passively conformed to a wide range of object shapes [10]. Though these grippers vary in method and application, they suffer from a common limitation: in order to be effective, the target must be placed such that its preferred axis is horizontal, the vehicle must descend directly down to the object so that its approach direction is vertical, the vehicle must make an approach perpendicular to the plane of the target, and the approach velocity must be close to zero when grasping. The ingressive gripper in [11] was able to perch with more aggressive trajectories by triggering a spring-loaded claw that would engage upon contact, but still needed to contact the target surface with a normal velocity.

Video analysis of birds of prey, such as the Bald Eagle (*Haliaeetus leucocephalus*) shown in Fig. 1, reveal that an Eagle sweeps its legs and claws backwards during its capture phase, thereby reducing the relative velocity between the claws of the predator and the prey [7]. This allows the bird to have a near-zero relative velocity of the claw while grasping its desired target without slowing down. This strategy provides a high rate of success in grasping prey, even though most fish can maneuver quickly out of harm's way if they can detect the predator far enough in advance. We draw inspiration from this to enable high-speed aerial grasping and manipulation.

The rest of the paper is structured as follows. We first present a novel gripper design that enables changing the relative velocity of the gripper with respect to a quadrotor MAV. Next, we present the dynamic model of the quadrotor MAV equipped with the gripper, and we demonstrate that the system is differentially flat. Following this, we present trajectory generation based on the flat outputs and an overview of the controller used. The next section presents experimental results of high-speed grasping at 2 m/s and 3 m/s, and a nondimensional comparison of the MAV trajectories with that of an avian trajectory. Finally, we present concluding remarks with thoughts for future work.

DESIGN OF A DUAL ARTICULATED GRIPPER

Gripper design is critical for high-speed aerial manipulation. A primary goal of a successful gripper is to enable MAVs to acquire payloads while moving at significant relative velocities. A secondary goal is to enable the ability to perch by compliantly grasping arbitrary-shaped objects or features such as tree branches or roof tops that are available in typical urban environments.

An initial gripper design resembled a two-pronged fork that interfaces with a plastic ball fixed to the payload, as seen in Fig. 2. The fork is 3D printed from Acrylonitrile Butadiene Styrene (ABS) and is designed to guide the ball into a spherical recess where it remains secure. A quadrotor equipped with this claw can acquire payloads at relative speeds up to 1 m/s. To release the payload, the fork can be separated by a mini servo motor. However, this method of deployment requires specialized fixtures on the payload, and it is incapable of robustly grasping objects at higher speeds due to larger relative speeds between the gripper and the object to be gripped.

To enable more flexible grippers, the finger design used in [12] is adapted for the quadrotor platform. A similar mechanism

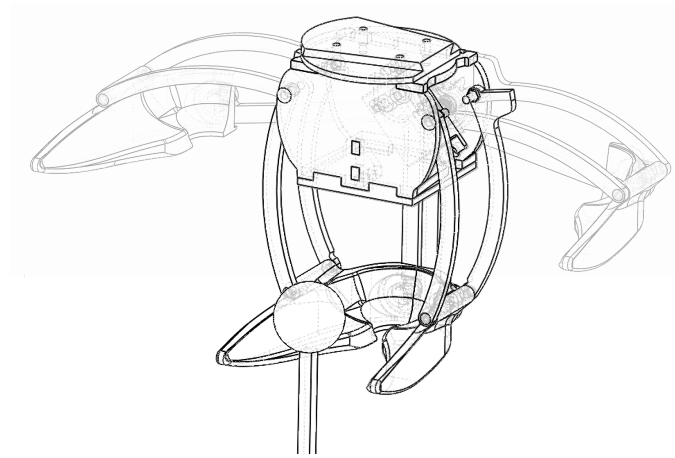

FIGURE 2. AN EARLY PROTOTYPE GRIPPER THAT COULD BE USED WITH SPHERICAL TARGETS. UNFORTUNATELY, THE GRIPPER WAS NOT PARTICULARLY SUCCESSFUL IN RETRIEVING NON SPHERICAL OBJECTS. THE GRIPPER IS SHOWN IN ITS OPEN (SHADED) AND CLOSED (SOLID) CONFIGURATIONS.

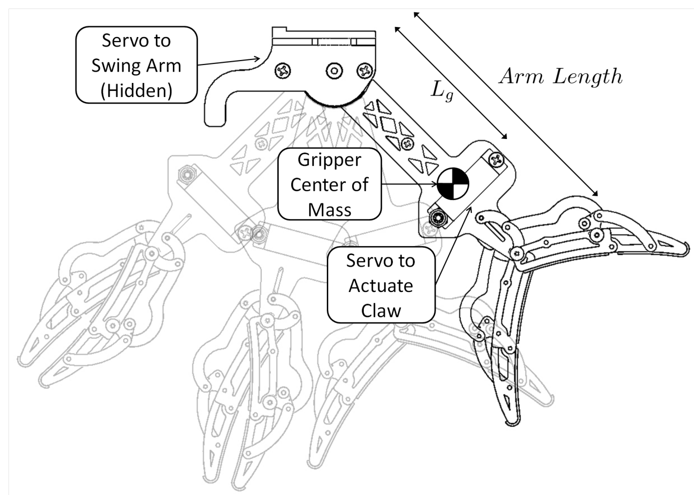

FIGURE 3. THE GRIPPER ARM IN MOTION AS THE CLAW IS GRASPING. THE SHADED PROJECTIONS DEMONSTRATE THE MOTION AS THE ARM SWINGS ABOUT THE AXIS POINTED INTO THE PAGE.

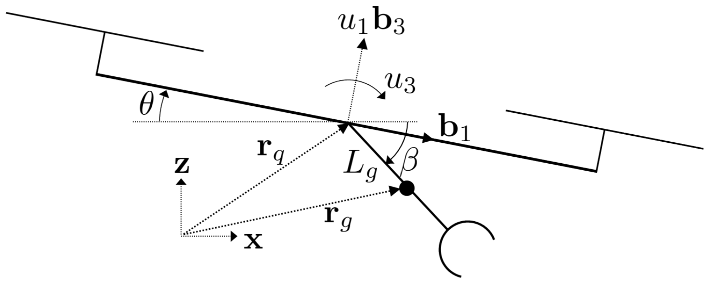

FIGURE 4. THE QUADROTOR HAS CONTROL INPUTS u_1 IN THE $\mathbf{b}_3$ DIRECTION AND u_3 AS A MOMENT ABOUT THE AXIS INTO THE PAGE. THE GRIPPER FORMS THE ANGLE β WITH THE HORIZONTAL AND ITS CENTER OF MASS IS LOCATED A DISTANCE L_g AWAY FROM THE QUADROTOR'S CENTER OF MASS.

is studied in [13]. As a result of our actuation design, all three fingers conform to the object shape while being collectively driven by a single servo motor. The fingers are constructed from laser-cut ABS and covered with Dycem, a high-friction rubber that is used to improve grip. Although this design facilitates the grasping of arbitrary object shapes, the fingers alone cannot close fast enough to capture payloads if the quadrotor is in motion.

Next, to reduce the relative speed between the gripper and the object to be gripped, we draw inspiration from the way an Eagle sweeps its legs just prior to grasping. In particular, the passively actuated gripper that is developed is mounted on a rotating arm of length 10.5 cm. The arm, also composed of laser-cut ABS, pivots directly below the quadrotor's center of mass and is actuated by a mini servo motor. When the arm rotates, the gripper experiences a tangential velocity that reduces the relative speed between itself and the payload during flight. See Fig. 3 for a time-lapse visualization of the motion.

This gripper design satisfies our goals of enabling high-speed grasping, while also compliantly grasping arbitrarily shaped objects. This can be further improved in the future by leveraging shape deposition manufacturing (SDM) methods for fabricating light-weight fingers [14], which will permit acquisition at even faster speeds.

DYNAMICAL MODEL AND DIFFERENTIAL FLATNESS

We develop a dynamical model for a quadrotor MAV equipped with an articulated gripper. The dynamics of a quadrotor platform are well-documented [15, 16], and involve a net thrust, u_1, in the direction perpendicular to the plane of the body and moments u_2, u_3, and u_4 acting along three body axes, $\mathbf{b}_1$, $\mathbf{b}_2$, and $\mathbf{b}_3$, respectively. In this paper, we adopt a planar version of this model for two reasons. First, in most examples of avian grasping and perching, the significant movements are limited to the sagittal plane of the bird. Indeed most of the examples of claws and feet seen in nature have an axis of symmetry. Second, it is difficult to achieve high speed grasping without specifying a plane of approach. Note that most previous work requires the approach to be restricted to a single direction. Thus, we develop a simplified dynamic model, in which we only consider the motion in the x-z plane with only two inputs, u_1 and u_3. See Fig. 4 for a visualization.

The angle of the gripper relative to the horizontal (x-axis) is defined as β, as displayed in Fig. 4, and the attitude of the vehicle is defined by θ, such that the angle between the quadrotor and the gripper is $\gamma = \beta - \theta$. Further, the masses of the quadrotor and gripper are defined as m_q and m_g, respectively, while the moments of inertia about the center of mass of the planar quadrotor and gripper are defined as J_q and J_g, respectively. Since the axis of rotation for the gripper is assumed to be at the quadrotor's center of mass, the fixed distance L_g denotes the length from the gripper's center of mass to the quadrotor's center of mass. We express the position vector of the quadrotor and gripper as $\mathbf{r}_q = \begin{bmatrix} x_q & z_q \end{bmatrix}^T$ and $\mathbf{r}_g = \begin{bmatrix} x_g & z_g \end{bmatrix}^T$, respectively.

The position of the gripper is entirely determined from the position of the quadrotor and the angle of the gripper through

$$\mathbf{r}_g = \mathbf{r}_q + L_g \begin{bmatrix} \cos(\beta) \\ -\sin(\beta) \end{bmatrix}. \tag{1}$$

Furthermore, higher-order time-derivatives of the gripper position can also be expressed as functions of the position of the quadrotor, the angle of the gripper, and their higher-order derivatives.

Dynamics

The dynamics are determined using Lagrangian mechanics where the potential energy is

$$V = m_q g z_q + m_g g z_g, \tag{2}$$

and the kinetic energy is

$$T = \frac{1}{2}\left(m_g \left\|\dot{\mathbf{r}}_g\right\|_2^2 + m_q \left\|\dot{\mathbf{r}}_q\right\|_2^2 + J_g \omega_g^2 + J_q \omega_q^2 \right). \tag{3}$$

Then, $\mathbf{q} = \begin{bmatrix} x_q & z_q & \theta & \beta \end{bmatrix}^T$ is the vector of generalized coordinates so that the corresponding active forces and moments are

$$\mathbf{F} = \begin{bmatrix} u_1 \sin(\theta) \\ u_1 \cos(\theta) \\ u_3 - \tau \\ \tau \end{bmatrix}, \tag{4}$$

where τ is the actuator torque on the gripper arm.

The inertial forces and moments are determined using the Euler-Lagrange equation so that the dynamics are given by

$$\ddot{\mathbf{q}} = D^{-1}\left(\mathbf{F} - C\dot{\mathbf{q}} - G\right) \tag{5}$$

where the matrices D, C, G are defined as

$$D = \begin{bmatrix} m_g + m_q & 0 & 0 & -L_g m_g s(\beta) \\ 0 & m_g + m_q & 0 & -L_g m_g c(\beta) \\ 0 & 0 & J_q & 0 \\ -L_g m_g s(\beta) & -L_g m_g c(\beta) & 0 & J_g + L_g^2 m_g \end{bmatrix}, \tag{6}$$

$$C = \begin{bmatrix} 0 & 0 & 0 & -L_g m_g c(\beta)\dot{\beta} \\ 0 & 0 & 0 & L_g m_g s(\beta)\dot{\beta} \\ 0 & 0 & 0 & 0 \\ 0 & 0 & 0 & 0 \end{bmatrix}, \tag{7}$$

$$G = \begin{bmatrix} 0 \\ g(m_g + m_q) \\ 0 \\ -g L_g m_g c(\beta) \end{bmatrix}, \tag{8}$$

with $s(\beta) = \sin(\beta)$, and $c(\beta) = \cos(\beta)$.

Differential Flatness

The dynamical model will serve for validation of controllers in simulation. However, to enable planning high-speed dynamic trajectories for aerial grasping, we will demonstrate that the system under consideration is differentially flat [17, 18]. Differential flatness has been used to plan aggressive trajectories for quadrotor systems [16], and we will take a similar approach. Showing that the system is differentially flat and identifying the flat outputs allows trajectory planning which guarantees feasibility while minimizing control inputs.

A system is differentially flat if there exists a change of coordinates which allows the state, $(\mathbf{q}, \dot{\mathbf{q}})$, and control inputs, $\mathbf{u}$, to be written as functions of the flat outputs and their derivatives $(y_i, \dot{y}_i, \ddot{y}_i, ...)$ [18]. Additionally, we require that the flat outputs are functions of the state and the control inputs [18]. If the change of coordinates is a diffeomorphism, we can plan trajectories using the flat outputs and their derivatives in the flat space since there is a unique mapping to the full state space of the dynamic system.

We will show that the flat outputs for the quadrotor-gripper coupled system are

$$\mathbf{y} = \begin{bmatrix} x_q & z_q & \beta \end{bmatrix}^T. \tag{9}$$

Defining $m_s = m_q + m_g$, the center of mass of the coupled system is

$$\mathbf{r}_s = \frac{m_q \mathbf{r}_q + m_g \mathbf{r}_g}{m_s}. \tag{10}$$

We recall from (1) that $\mathbf{r}_q =: f_1(y_1, y_2)$ and $\mathbf{r}_g =: f_2(y_1, y_2, y_3)$. Thus, $\mathbf{r}_s =: f_3(y_1, y_2, y_3)$ and $\ddot{\mathbf{r}}_s = \ddot{f}_3$. Defining $\mathbf{e}_3$ as the third standard basis vector, the three-dimensional Newtonian equations of motion are

$$m_s \ddot{\mathbf{r}}_s = u_1 \mathbf{b}_3 - m_s g \mathbf{e}_3 \tag{11}$$

revealing that

$$u_1 = m_s \left\| \ddot{\mathbf{r}}_s + g\mathbf{e}_3 \right\| \tag{12}$$

and

$$\mathbf{b}_3 = \frac{\ddot{\mathbf{r}}_s + g\mathbf{e}_3}{\left\| \ddot{\mathbf{r}}_s + g\mathbf{e}_3 \right\|} \tag{13}$$

from which θ can be determined. In addition, (13) requires that $\|\ddot{\mathbf{r}}_s + g\mathbf{e}_3\| > 0$ or that $u_1 > 0$. Since the system is restricted to the planar case, $\mathbf{b}_2 = \mathbf{e}_2$ and $\mathbf{b}_1 = \mathbf{b}_2 \times \mathbf{b}_3$. Next, we differentiate (11) to obtain

$$m_s \dddot{\mathbf{r}}_s = \dot{u}_1 \mathbf{b}_3 + \Omega \times u_1 \mathbf{b}_3 \tag{14}$$

where $\Omega = \dot{\theta}\mathbf{b}_2$. The projection onto $\mathbf{b}_3$ reveals

$$\dot{u}_1 = \mathbf{b}_3 \cdot m_s \dddot{\mathbf{r}}_s \tag{15}$$

and, using this relationship,

$$\Omega \times \mathbf{b}_3 = \frac{m_s}{u_1}\left(\dddot{\mathbf{r}}_s - (\mathbf{b}_3 \cdot \dddot{\mathbf{r}}_3)\mathbf{b}_3\right). \tag{16}$$

We notice that this is purely in the $\mathbf{b}_1 - \mathbf{b}_2$ plane and, more specifically, that $\Omega \times \mathbf{b}_3 = \dot{\theta}\mathbf{b}_1$ Thus,

$$\dot{\theta} = \frac{m_s}{u_1}\left(\mathbf{b}_1 \cdot \dddot{\mathbf{r}}_s\right). \tag{17}$$

Next, we take the second derivative of (11) to obtain

$$\begin{aligned} m_s \mathbf{r}_s^{(4)} = {} & \dot{u}_1 \dot{\theta}\mathbf{b}_2 \times \mathbf{b}_3 + \ddot{u}_1 \mathbf{b}_3 + \dot{\theta}\mathbf{b}_2 \times \dot{u}_1 \mathbf{b}_3 \\ & + \dot{\theta}\mathbf{b}_2 \times \left(\dot{\theta}\mathbf{b}_2 \times u_1 \mathbf{b}_3\right) + \ddot{\theta}\mathbf{b}_2 \times u_1 \mathbf{b}_3. \end{aligned} \tag{18}$$

Collecting terms and simplifying cross products,

$$m_s \mathbf{r}_s^{(4)} = \left(2\dot{u}_1\dot{\theta} + \ddot{\theta}u_1\right)\mathbf{b}_1 + \left(\ddot{u}_1 - \dot{\theta}^2 u_1\right)\mathbf{b}_3. \tag{19}$$

The projections onto $\mathbf{b}_1$ and $\mathbf{b}_3$ reveal

$$\ddot{\theta} = \frac{1}{u_1}\left(m_s \mathbf{b}_1 \cdot \mathbf{r}_s^{(4)} - 2\dot{u}_1\dot{\theta}\right) \tag{20}$$

and

$$\ddot{u}_1 = \mathbf{b}_3 \cdot \left(m_s \mathbf{r}_s^{(4)}\right) + \dot{\theta}^2 u_1. \tag{21}$$

Next, we let F_x and F_z be reaction forces at the attachment point of the gripper so that the translational and angular equations of motion of the gripper are

$$m_g \ddot{x}_g = F_x \tag{22}$$
$$m_g \ddot{z}_g = F_z - m_g g \tag{23}$$
$$J_g \ddot{\beta} = \tau + F_x L_g \sin(\beta) + F_z \cos(\beta). \tag{24}$$

Solving for the gripper arm actuator torque, τ,

$$\tau = J_g \ddot{\beta} - L_g m_g \left(\ddot{x}_g \sin(\beta) + (\ddot{z}_g + g)\cos(\beta)\right). \tag{25}$$

Lastly, we know that

$$u_3 = \ddot{\theta} J_q + \tau. \tag{26}$$

Thus, we have demonstrated that the state and the inputs of the coupled system are functions of the flat outputs and their derivatives, establishing that the system is differentially flat. This allows us to plan trajectories in the space of flat outputs, which automatically yield the feed-forward control inputs required to follow the planned trajectory. Further, since the control inputs are functions of the snap $\left(\mathbf{r}^{(4)}\right)$ of the trajectory, trajectories planned in the flat space must be continuous and differentiable in the position $(\mathbf{r})$, velocity $(\dot{\mathbf{r}})$, acceleration $(\ddot{\mathbf{r}})$, and jerk $(\dddot{\mathbf{r}})$.

TRAJECTORY GENERATION AND CONTROL DESIGN

From the previous section, further examination of the control inputs reveals that the snap of the position of the quadrotor appears in the u_3 term through $\ddot{\theta}$. To minimize the norm of the input vector, it is meaningful to minimize a cost functional constructed from the trajectory snap. Accordingly we consider minimal snap trajectories, which can be generated by following a Quadratic Programming (QP) approach, as used in [16]. Further examination reveals the same for β.

Although we have a method to generate trajectories for the quadrotor, we do not have a definitive way to determine the constraints for the trajectory. For this, we take inspiration from nature and analyze video footage of an Eagle grasping a fish out of water. The segment of video used is from a static frame at an unknown distance and unknown time-scale since the video segment is in slow motion. The extracted trajectory will be compared later in a following section.

The trajectories used for experimentation are constrained by position at the start and finish where the higher derivatives are zero. In addition, the position at pickup is specified, but the velocity, acceleration, and jerk are free and are required to be continuous. A fully-defined trajectory was planned for the x and z positions of the quadrotor. Using these, discrete position constraints were placed on β during the time preceding pickup $(t_p - 400ms, t_p - 200ms)$ and at the time of pickup (t_p) so that the gripper would be pointed directly at the target. See Fig. 5 and Fig. 6 for a desired and experimental trajectory for the position and the gripper angle, respectively.

Next, we briefly present the controller that drives the quadrotor and gripper system along the designed nominal trajectory. The quadrotor controller has an outer position control loop running at 100Hz which generates a desired attitude and feedforward control inputs. An inner PD attitude control loop running

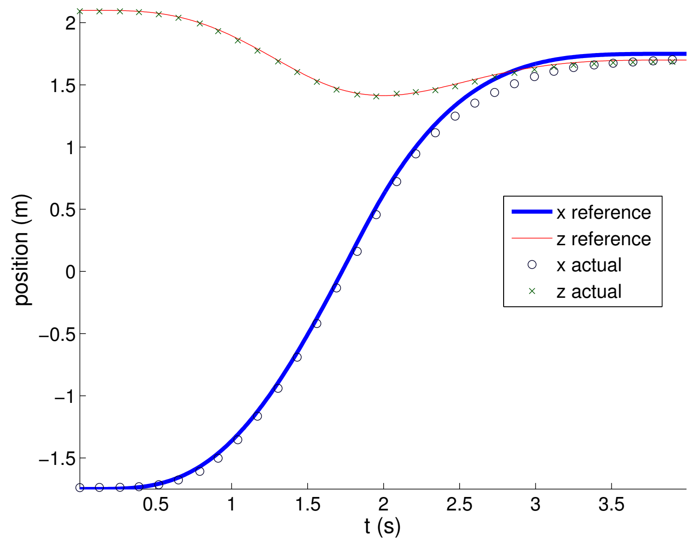

FIGURE 5. NOMINAL (PLANNED) QUADROTOR POSITION TRAJECTORIES OVERLAYED WITH EXPERIMENTAL RESULTS. THE PLANNED PICKUP TIME IS $t = 2s$.

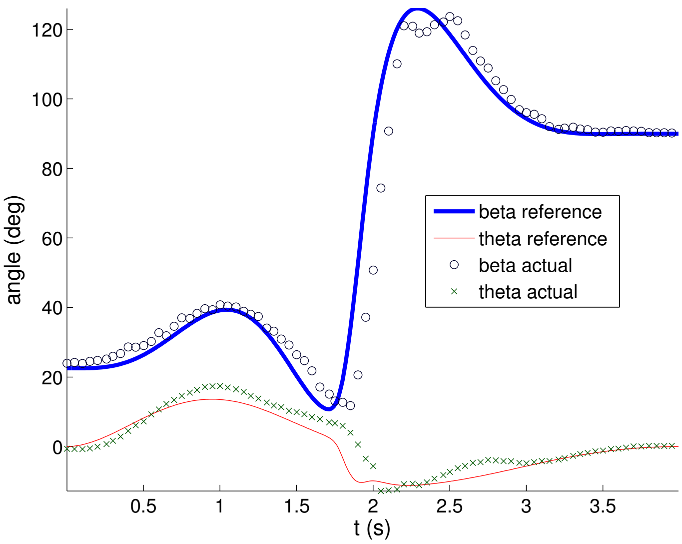

FIGURE 6. NOMINAL (PLANNED) β AND θ TRAJECTORIES OVERLAYED WITH EXPERIMENTAL RESULTS. THE PLANNED PICKUP TIME IS $t = 2s$.

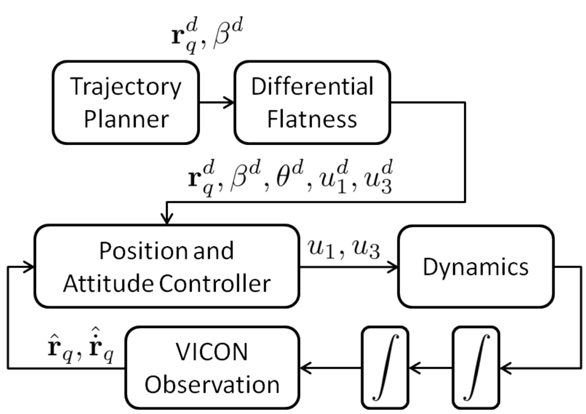

FIGURE 7. A BLOCK DIAGRAM OF THE CONTROLLER USED FOR EXPERIMENTS. A SUPERSCRIPT "d" DENOTES A DESIRED OR NOMINAL VALUE AND A HAT INDICATES AN ESTIMATE.

at 1Khz is used to drive the robot to the desired attitude. The position and attitude controllers are based on the quadrotor hover controller in [5] and the feedforward control input serves to compensate for the motion of the gripper. The state of the quadrotor is observed using VICON and feedforward control inputs are supplied to the outer position control loop as displayed in Fig. 7.

RESULTS

We demonstrate experimental results on an Asctec Hummingbird quadrotor [19], weighing 500 gm, and equipped with a

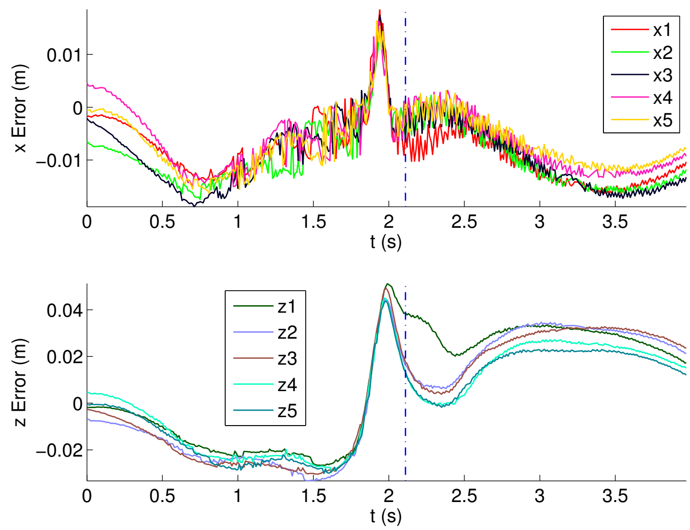

FIGURE 8. THE ERRORS OF THE GRIPPER FOR 5 CONSECUTIVE TRIALS. THE ACTUAL PICKUP TIME IS SLIGHTLY AFTER $t = 2s$ AND IS REPRESENTED BY A VERTICAL LINE.

gripper weighing 158 gm. The experiments utilize the GRASP Multiple Micro UAV Testbed [15] and leverage a motion capture system to accurately determine the state of the quadrotor [20]. A 27 gm cylindrical target was tracked using VICON [20].

The controller presented in the earlier section, that combines feedforward control inputs and a simple PD feedback controller on the quadrotor was used in experiments, and the gripper claw was commanded to close slightly before the pickup time. With this setup, the quadrotor grasped the target while moving at 2 m/s with a success rate of 100% out of 5 attempts. Position errors for those trajectories are presented in Fig. 8. The quadrotor was able to successfully grasp the target at speeds up to 3 m/s, or 9 body lengths / s (Fig. 11).

Avian Comparison

In assessing the success of our results, it seems appropriate to use the Eagle's performance as a standard of comparison. We desire the same end result that the Eagle achieves, and therefore expect to match the bird closely.

The footage of the Eagle is slowed by an unknown factor resulting in an unknown time scale. The length scale is also impossible to extract accurately. However, it is still meaningful to compare the two nondimensionalized sets of trajectories. We nondimensionalize the trajectories using the following relationships:

$$x^\star = \frac{x}{L}, \quad z^\star = \frac{z}{L}, \quad t^\star = \frac{t v_p}{L} \tag{27}$$

TABLE 1. UNITS OF NON-DIMENSIONALIZATION FACTORS

	BIRD TRAJECTORY FROM VIDEO FOOTAGE	ROBOT TRAJECTORY ESTIMATED FROM VICON MEASUREMENTS
L_g	pixels	meters
v_p	pixels/frame	meters/sec

where v_p is the velocity at pickup and L is the length from the axis of rotation to the gripping surface. The units are detailed in Table 1. Results using this approach are presented in Figs. 9 and 10. It can be seen that the x-position of the gripper followed closely to that of the Eagle's claws. The significant deviation in z-position following pick-up can be attributed to the limited range of motion of the arm of the quadrotor compared to that of the Eagle. Furthermore, the nondimensionalized length of the quadrotor's arm is slightly less than that of the fully extended Eagle's leg. If the body length was used as the characteristic length, the gripper arm has a nondimensionalized length of 0.31 compared to the Eagle's leg at 0.45. The length of the gripper arm was limited by weight constraints.

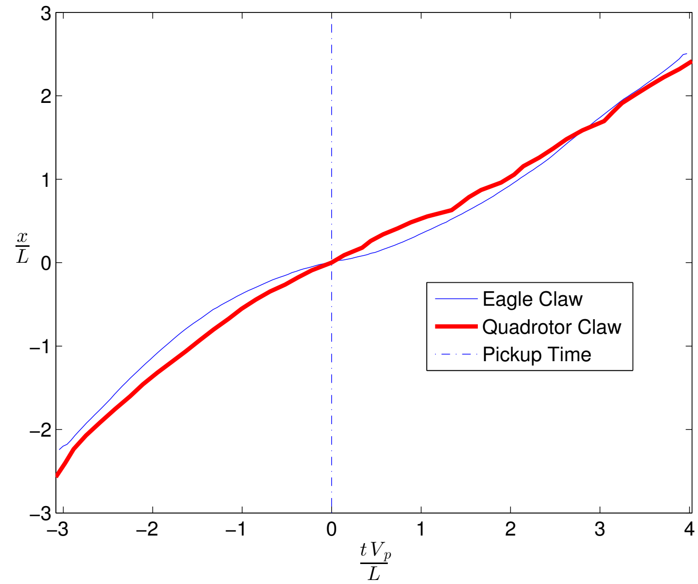

FIGURE 9. A COMPARISON OF THE NON-DIMENSIONALIZED x POSITIONS OF THE QUADROTOR CLAW AND THE EAGLE CLAW. THE LOWEST POINT ON z IS CONSIDERED THE PICKUP POINT AND IS DENOTED BY THE VERTICAL LINE. THE EAGLE CLAW HAS A SLOWER RELATIVE VELOCITY AT PICKUP THAN OUR CLAW WHEN THE QUADROTOR BODY SPEED IS 2 m/s.

CONCLUSION AND FUTURE WORK

In this paper, we explored the challenges of high-speed aerial grasping using a quadrotor UAV equipped with a gripper. A novel appendage design, inspired by the articulation of an Eagle's legs and claws, was shown enable a high rate of success while grasping objects at fast speeds. The dynamical model of the quadrotor and gripper system was shown to be differentially flat, and minimum snap trajectories were generated for dynamic pickup. Experimental results were presented for grasping objects between 2 m/s and 3 m/s (6 - 9 body lengths per second. Finally, preliminary comparisons of the nondimensionalized quadrotor's trajectories with corresponding avian trajectories were found to be encouraging.

There are three directions for future research. First, we aim to accomplish the same end results without using the Vicon motion capture system. This can be done by incorporating visual servoing algorithms in which the errors between the desired target position and actual position in the retina drive the robot. Just as an Eagle is able to navigate based only on its own visual and inertial sensors, a quadrotor should be able to make in-flight corrections using data from an on-board camera. Another direction of research is autonomous detection of candidate sites for perching and controlled landing on perching sites. Resting on a stationary fixture is highly preferable to hovering to minimize energy usage and noise. Finally, we will pursue SDM based designs to create appendages with lower inertia which in turn will enable more agile grasping and perching strategies.

REFERENCES

[1] Lindsey, Q., Mellinger, D., and Kumar, V., 2011. "Construction of Cubic Structures with Quadrotor Teams". In Proceedings of Robotics: Science and Systems.

[2] Sreenath, K., Michael, N., and Kumar, V., 2013. "Trajectory Generation and Control of a Quadrotor with a Cable-Suspended Load A Differentially-Flat Hybrid System". In ICRA.

[3] Mellinger, D., Shomin, M., Michael, N., and Kumar, V., 2010. "Cooperative grasping and transport using multiple quadrotors". In Proceedings of the International Symposium on Distributed Autonomous Robotic Systems.

[4] Venable, N., 1996. *Birds of Prey*. West Virginia University Extension Service.

[5] Mellinger, D., Michael, N., and Kumar, V., 2010. "Trajectory Generation and Control for Precise Aggressive Maneuvers with Quadrotors". In Proceedings of the International Symposium on Experimental Robotics.

[6] Kumar, V., and Michael, N., 2011. "Opportunities and chal-

FIGURE 11. A STILL IMAGE COMPARISON BETWEEN THE EAGLE AND THE QUADROTOR FOR A TRAJECTORY WITH THE QUADROTOR MOVING AT 3 m/s (9 BODY LENGTHS / s) AT PICKUP.

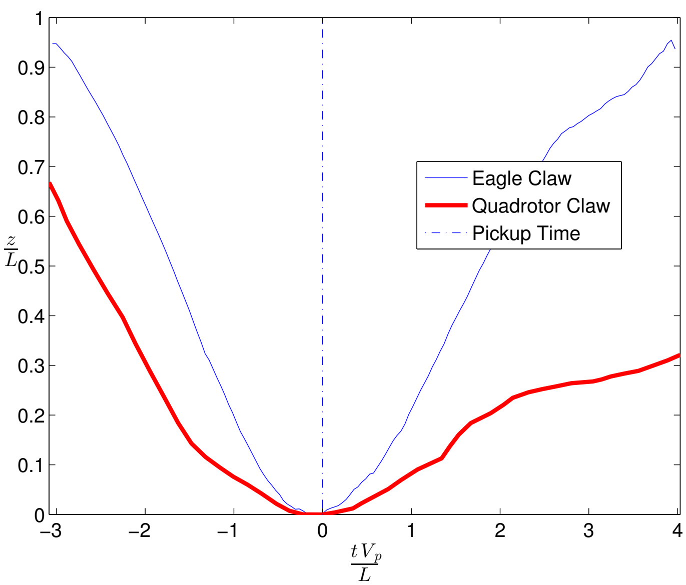

FIGURE 10. A COMPARISON OF THE NON-DIMENSIONALIZED z POSITIONS OF THE QUADROTOR AND THE EAGLE CLAW. THE VERTICAL LINE INDICATES THE PICKUP TIME.

lenges with autonomous micro aerial vehicles". *Int. Symp. on Robotics Research*, pp. 1–16.

[7] Bass, K., Leith, B., Anderson, J., Bassett, P., Stevens, J., Pearson, H., and Turner, J., 2009. Nature's Most Amazing Events. [DVD]. BBC Worldwide Ltd. Programs.

[8] Doyle, C. E., Bird, J. J., Isom, T. A., Johnson, C. J., Kallman, J. C., Simpson, J. A., King, R. J., Abbott, J. J., and Minor, M. A., 2011. "Avian-inspired passive perching mechanism for robotic rotorcraft". In 2011 IEEE/RSJ International Conference on Intelligent Robots and Systems, IEEE, pp. 4975–4980.

[9] Mellinger, D., Lindsey, Q., Shomin, M., and Kumar, V., 2011. "Design, modeling, estimation and control for aerial grasping and manipulation". In Intelligent Robots and Systems (IROS), 2011 IEEE/RSJ International Conference on, IEEE, pp. 2668–2673.

[10] Dollar, A. M., and Howe, R. D., 2010. "The Highly Adaptive SDM Hand: Design and Performance Evaluation". *The International Journal of Robotics Research,* ***29***(5), Feb., pp. 585–597.

[11] Mellinger, D., Shomin, M., and Kumar, V., 2010. "Control of Quadrotors for Robust Perching and Landing". In Proceedings of the International Powered Lift Conference.

[12] Festo Coorporate. ExoHand, from http://www.festo.com/cms/en_corp/12713.htm.

[13] Dollar, A. M., and Howe, R. D., 2011. "Joint coupling design of underactuated hands for unstructured environments". *The International Journal of Robotics Research,* ***30***(9), June, pp. 1157–1169.

[14] Dollar, A., and Howe, R., 2006. "A robust compliant grasper via shape deposition manufacturing". *IEEE/ASME Transactions on Mechatronics,* ***11***(2), Apr., pp. 154–161.

[15] Michael, N., Mellinger, D., Lindsey, Q., and Kumar, V., 2010. "The GRASP multiple micro-UAV testbed". *Robotics & Automation Magazine, IEEE,* ***17***(3), pp. 56–65.

[16] Mellinger, D., and Kumar, V., 2011. "Minimum snap trajectory generation and control for quadrotors". In 2011 IEEE International Conference on Robotics and Automation, IEEE, pp. 2520–2525.

[17] Fliess, M., Levine, J., Martin, P., and Rouchon, P., 1995. "Flatness and defect of non-linear systems: introductory theory and examples". *International Journal of Control,* ***61***(6), June, pp. 1327–1361.

[18] Murray, R., Rathinam, M., and Sluis, W., 1995. "Differ-

ential flatness of mechanical control systems: A catalog of prototype systems". In Proceedings of the 1995 ASME International Congress and Exposition, Citeseer.
[19] Ascending Technologies GmbH.
[20] Vicon Motion Capture System.